MAP COMPUTATION FROM MAGNETIC FIELD DATA AND APPLICATION TO THE LHC HIGH-GRADIENT QUADRUPOLES

M. Venturini, D. Abell, and A. Dragt,
Physics Department, University of Maryland, College Park MD 20742 USA

Abstract

In many cases the most accurate information about fields in a magnet comes either from direct measurement or from a numerical computation done with a 3D electromagnetic code. In this paper we show how this information can be used to compute transfer maps with high accuracy. The resulting transfer maps take into account all effects of real beamline elements including fringe-field and multipole error effects. The method we employ automatically incorporates the smoothing properties of the Laplace Green function. Consequently, it is robust against both measurement and electromagnetic code errors. As an example, we apply the method to a study of end effects in the High-Gradient quadrupoles for the low-beta insertion in the Large Hadron Collider (LHC). The map computation for the quadrupoles has been carried out using MARYLIE's GENMAP routine and a newly written MARYLIE user-defined routine. For long-term tracking we used Cremona symplectification techniques as implemented in CTRACK.

1 INTRODUCTION

The motion of charged particles through any beam-line element is described by the transfer map $\mathcal{M}$ for that element. Through aberrations of order $(n-1)$ such a map has the Lie representation [1, 2]

$$\mathcal{M} = \mathcal{R}_2 \exp(:f_3:) \exp(:f_4:) \cdots \exp(:f_n:). \qquad (1)$$

The linear map $\mathcal{R}_2$ and the Lie generators f_ℓ are determined by the equation of motion $\dot{\mathcal{M}} = \mathcal{M} : -H :$ where $H = H_2 + H_3 + H_4 + \cdots$ is the Hamiltonian expressed in terms of deviation variables and expanded in a homogeneous polynomial series. The deviation variable Hamiltonian H is determined in turn by the Hamiltonian K. In Cartesian coordinates with z taken as the independent variable, and in the absence of electric fields, K is given by the relation

$$K = -[p_t^2/c^2 - m^2c^2 - (p_x - qA_x)^2 - (p_y - qA_y)^2]^{1/2} - qA_z.$$

Here $\boldsymbol{A}$ is the magnetic vector potential. We therefore need a Taylor expansion for the vector potential components A_x, A_y, A_z in the deviation variables x and y. How can the coefficients of the Taylor expansion for the vector potential be determined from a knowledge of the magnetic field? In this paper we review the method we proposed in [3] and present an application to the High-Gradient quadrupoles in the interaction region of the LHC. The method uses information about the fields coming from either direct measurement or numerical computation done with a 3D electromagnetic code. It is based on the calculation of Fourier integrals with suitable kernels derived from the Green function of the Laplace equation. Our approach is different from and more accurate than other methods based on numerical differentiation (see [4]). A pleasant feature is relative insensitivity to the presence of noise in the magnetic field data, which makes the method capable of providing accurate computations of high order terms in the desired Taylor expansion. An additional advantage is that it applies, with minor modifications, to both magnet data obtained by numerical computation and measured data found with spinning coils (see [3, 5] for more details on this aspect). A similar approach is also followed in [6].

2 DETERMINATION OF THE VECTOR POTENTIAL

In a current-free region the magnetic field $\boldsymbol{B}$ can be described most simply in terms of a *scalar* potential ψ (with $\boldsymbol{B} = \nabla\psi$) obeying the Laplace equation $\nabla^2\psi = 0$. In cylindrical coordinates the general solution to this equation (that is regular for small ρ) has the expansion

$$\psi = \sum_{m=0}^{\infty} \int_{-\infty}^{\infty} dk e^{ikz} I_m(k\rho) \times [\hat{b}_m(k) \sin m\phi + \hat{a}_m(k) \cos m\phi], \qquad (2)$$

where the functions $\hat{a}_m(k)$ and $\hat{b}_m(k)$ are arbitrary, and I_m is the modified Bessel function. This is a "cylindrical multipole" expansion, where m is related to the order of the multipole, and should not be confused with a spherical multipole expansion. The first term on the RHS of (2) describes a purely solenoidal field ($m = 0$). The other terms in the series correspond to the dipole $(m = 1)$, quadrupole $(m = 2)$, $\cdots$ components. For simplicity we will treat the terms with $m \geq 2$. The solenoidal term requires a separate, but analogous, treatment that entails no new complications. The dipole case is more complicated. In the sometimes restrictive case that the sagitta of the design orbit does not exceed the radius R introduced in Sec. 3, the methods of this paper also apply. However other methods are required if the sagitta is larger.

If ψ is given in the form (2), a suitable corresponding vector potential is easily found. Since there is gauge freedom, a possible covenient choice, in the absence of a solenoidal component, is to work in a gauge satisfying $A_\phi = 0$. Suppose ψ as given by (2) is rewritten in the form

$$\psi = \sum_{m=1}^{\infty} \psi_{m,s}(\rho, z) \sin m\phi + \psi_{m,c}(\rho, z) \cos m\phi \qquad (3)$$

with

$$\psi_{m,s}(\rho,z)=\int_{-\infty}^{\infty}dke^{ikz}I_m(k\rho)\hat{b}_m(k). \qquad (4)$$

[$\psi_{m,c}$ has the same form, with $\hat{a}_m(k)$ replacing $\hat{b}_m(k)$.] Then it is easily verified that the remaining components of the vector potential are given by the relations

$$\begin{aligned} A_\rho &= \sum_{m=1}^{\infty}\frac{\cos(m\phi)}{m}\rho\frac{\partial}{\partial z}\psi_{m,s}-\frac{\sin(m\phi)}{m}\rho\frac{\partial}{\partial z}\psi_{m,c},\\ A_z &= \sum_{m=1}^{\infty}-\frac{\cos(m\phi)}{m}\rho\frac{\partial}{\partial \rho}\psi_{m,s}+\frac{\sin(m\phi)}{m}\rho\frac{\partial}{\partial \rho}\psi_{m,c}. \end{aligned}$$

From the two equations above it is clear that finding Taylor expansions for the vector potential components A_x, A_y, and A_z (what we need) is equivalent to finding Taylor expansions for $\psi_{m,s}$ and $\psi_{m,c}$ in the variable ρ. This is easily done by a two-step process: first, we expand the modified Bessel functions $I_m(k\rho)$ appearing in (4) as Taylor series in the quantity $(k\rho)$. Doing so produces an expansion in powers of ρ with coefficients that involve integrations over various powers of k. Second, we observe that the powers of k can be replaced by multiple differentiation with respect to the variable z. The net results of these two steps are the relations $(\alpha=c,s)$

$$\psi_{m,\alpha}(\rho,z)=\sum_{\ell=0}^{\infty}(-1)^\ell\frac{m!}{2^{2\ell}\ell!(\ell+m)!}C_{m,\alpha}^{[2\ell]}(z)\rho^{2\ell+m}. \qquad (5)$$

The index $[2\ell]$ indicates the 2ℓ derivative with respect to the longitudinal variable z. The functions $C_{m,\alpha}^{[0]}(z)$ are the generalized on-axis gradients. Note that the generalized gradients depend on the longitudinal variable z. For fields produced by long well-made magnets, however, the z dependence will be significant only at the ends.

We conclude that the dynamics of a charged particle passing through a region of space occupied by a magnetic field described by the scalar potential (2) is completely determined by a knowledge of the generalized on-axis gradient functions $C_{m,\alpha}^{[0]}(z)$ and their derivatives. We will now describe two ways for computing the generalized gradients and their derivatives.

3 COMPUTATION OF GENERALIZED GRADIENTS FROM FIELD DATA

Suppose the radial component of the magnetic field B_ρ is known, either by measurement or computation, on the surface of some infinitely long cylinder of radius R. Moreover, suppose that the field is given in terms of an angular Fourier series,

$$B_\rho(\rho=R,\phi,z)=\sum_{m=1}^{\infty}B_m(R,z)\sin(m\phi)+A_m(R,z)\cos(m\phi).$$

It can be shown [5] that the generalized on-axis gradients appearing in the expansion coefficients for the scalar potential (8) can be written as

$$C_{m,s}^{[n]}(z)=\frac{i^n}{2^m m!}\frac{1}{\sqrt{2\pi}}\int_{-\infty}^{\infty}dke^{ikz}\frac{k^{m+n-1}}{I_m'(kR)}\tilde{B}_m(R,k). \qquad (6)$$

The expression for $C_{m,c}^{[n]}(z)$ has $\tilde{A}_m(R,k)$ replacing $\tilde{B}_m(R,k)$. Here $\tilde{B}_m(R,k)$ and $\tilde{A}_m(R,k)$ are the Fourier transforms of $B_m(R,z)$ and $A_m(R,z)$, *e.g.*,

$$\tilde{B}_m(R,k)=\frac{1}{\sqrt{2\pi}}\int_{-\infty}^{\infty}dze^{-ikz}B_m(R,z). \qquad (7)$$

In the case where the magnetic field is produced by an iron dominated magnet, and is therefore localized in space, the integrals (7) can be considered to have, in practice, finite limits of integration. With some care, an effective cut-off can also be found even if the fields extend to infinity since they fall off sufficiently rapidly at infinity. Also, since the generalized Bessel function $I_m'(w)$ increases exponentially for large $|w|$, there is also, in effect, a cut-off in k for the integral (6) defining the generalized gradients.

4 NUMERICAL TEST AND INSENSITIVITY TO ERRORS

The method described in Section 3 has been implemented in the code MARYLIE 5.0 [2] as a user-defined routine. The routine reads from an external file the functions $A_m(R,z)$ and $B_m(R,z)$, evaluated on a discrete set of points z_i. It then generates the corresponding transfer map by using the built-in routine GENMAP to integrate the map equation. Since MARYLIE 5.0 is a 5^{th} order code, only the multipoles through $m=6$ need be considered.

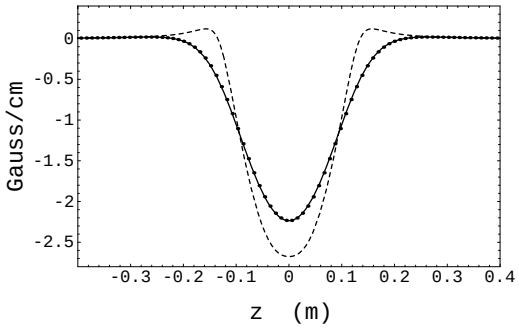

Figure 1: Plot of the scaled harmonic $B_2(R,z)/R$ (dashed line) and the on-axis gradient $2C_{2,s}^{[0]}(z)$ as calculated from surface data (dots) and analytically (solid line) for an ideal Lambertson quadrupole.

The integration algorithm of GENMAP is based on a 11^{th} order multistep (Adams) method. Because the algorithm uses a fixed step size, one needs to provide values of the generalized gradients and their derivatives only at the predetermined locations in z required by GENMAP.We

emphasize that no interpolation of the generalized gradients is required by GENMAP.

In order to test both the routines and the method we treated the case of an ideal iron-free Lambertson quadrupole. The use of this case as an example has the virtue that the various $C^{[n]}_{m,\alpha}(z)$ can also be determined analytically (see [5]). First we computed the surface data $B_\rho(\rho = R, \phi, z)$ using the Biot-Savart law, and made an angular Fourier analysis to calculate the harmonics $B_2(R,z)$ and $B_6(R,z)$ for various values of z, (because of the symmetries involved only the harmonics of order $m = 2, 6, 10...$ are non-vanishing). We set the radius R of the cylinder to be at 75% of the magnet aperture $r = 0.128$ m, with the length of the magnet being $2r$, and the step size Δz used in the calculation of the harmonics $= 6.44$ mm. Next, we used these data to reconstruct the multipole field expansion by applying our method and compared the results to those predicted by the analytic formulas.

Results are shown in Figs. 1 and 2. In Fig. 1 the dashed line is the function $B_2(R,z)/R$ as calculated numerically by using the Biot-Savart law. The solid line represents the on-axis gradient, which is equal to $2C^{[0]}_{2,s}(z)$, as calculated analytically, while the dots represent the same function as calculated from the surface data. The deviation between $B_2(R,z)/R$ and $2C^{[0]}_{2,s}(z)$ is due to terms in the multipole expansion containing derivatives of $2C^{[0]}_{2,s}(z)$. These terms are the so called pseudo-multipoles. This can be seen by writing the multipole expansion for B_ρ through 6^{th} order in ρ:

$$B_\rho = \left(2C^{[0]}_{2,s}\rho - \frac{1}{3}C^{[2]}_{2,s}\rho^3 + \frac{1}{64}C^{[4]}_{2,s}\rho^5\right)\sin 2\phi + 6C^{[0]}_{6,s}\rho^5 \sin 6\phi. \quad (8)$$

In Fig. 2, as an indication of the reliability of the method, we report the 8th derivative of the generalized gradient (needed for a 9^{th} order code) calculated from the surface data (dots) compared to the anlytical profile (solid line). The accuracy in the calculation of the generalized gradient is mirrored by the accuracy with which the elements of the transfer map can be determined. For this case we found relative errors ranging from 10^{-6} for $\mathcal{R}_2$ to 10^{-4} for f_5 and f_6.

In practical situations magnetic field data, whether coming from measurements or from numerical computations, are unavoidably affected by errors. What effect do these errors have on the determination of the generalized on-axis gradients and their derivatives? The effect of these errors is relatively mild. This relative insensitivity to errors arises from a basic property of solutions to Laplace's equation: the value of ψ at some interior point is an appropriately weighted average of its values over any surrounding boundary. Consequently, ψ is smoother in the interior of a region than it may be on a boundary of this region. Correspondingly, errors in boundary values are averaged. A way to see the smoothing mechanism in action is to look at (6) and observe the presence of the kernel $1/I'_m(kR)$ acting as a high frequency filter [$I'_m(kR)$ grows exponentially with kR]. Incidentally, note that for the purpose of noise reduction it is desirable to choose R as large as possible.

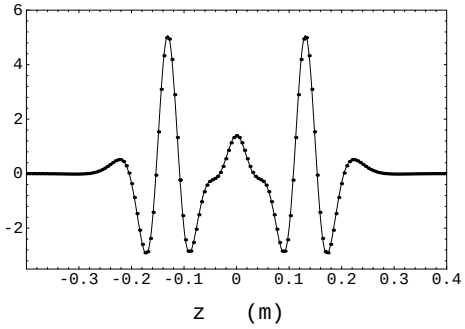

Figure 2: The function $C^{[8]}_{2,s}(z)$ (in units of 10^{-5} Gauss/cm^9) as calculated from surface data (dots) and analytically (solid line) for an ideal Lambertson quadrupole.

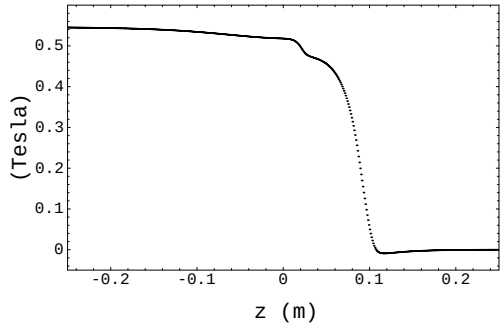

Figure 3: Harmonic $B_2(R,z)$ (quadrupole field component) for the Return End; R=3 cm.

We tested noise insensitivity by considering a simple noise model for which surface fields had values given by

$$B^{rnd}_2(R,z_i) = B_2(R,z_i)[1+\epsilon_2(z_i)], \quad (9)$$

and similarly for $B^{rnd}_6(R,z_i)$, where $\epsilon_2(z_i)$ is a random variable uniformly distributed in the interval $[-\epsilon/2, \epsilon/2]$, and $B_2(R,z_i)$ is the same as before. Then we calculated the generalized gradients and transfer map using the noisy data. For $\epsilon = 10^{-2}$ we found relative errors, ranging from 5×10^{-4} for $\mathcal{R}_2$ to 10^{-2} for f_5 and f_6, which are at worst on the order of the noise itself.

5 APPLICATION TO LHC HIGH-GRADIENT QUADRUPOLES

In this final Section we describe an application of our method to the calculation of the transfer maps for the High-Gradient (HG) superconducting quadrupoles located at the interaction region of LHC (see [8] and references therein). Our purpose here is two-fold: We want to *(i)* provide an illustration of the method in a case of physical interest and *(ii)* test the adequacy of the way magnets are usually modeled in tracking studies against our more realistic modeling.

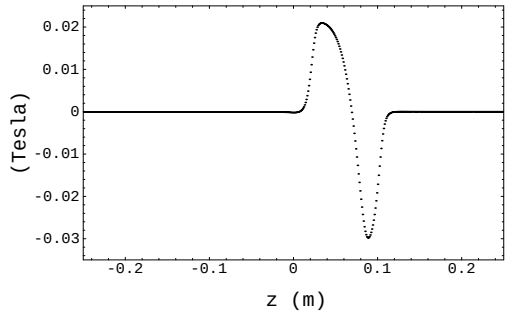

Figure 4: Harmonic $B_6(R,z)$ (duodecapole field component) for the Return End; R=3 cm.

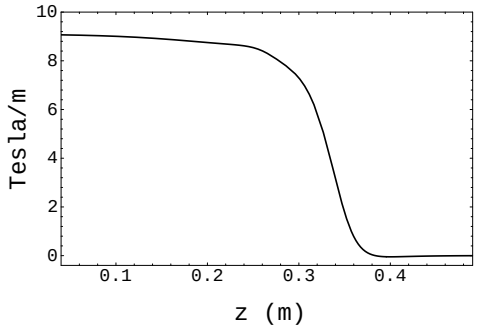

Figure 5: Generalized gradient $C_{2,s}(z)$ for the Return End. ($z = 25$ cm in this picture corresponds to $z = 0$ in Figs. 3 and 4.)

The HG quadrupoles provide the focusing necessary to compress the beam at each Interaction Points (IP) so as to enhance luminosity. This can be done only by allowing the beam to expand considerably in the regions adjacent to the IP's where the HG quadrupoles are located. As a result, the beam is particularly sensitive to the aberrations associated with the HG quadrupoles.

All the HG quadrupoles have same gradient (200.415 T/m) and are identical except for their lengths (details on the LHC lattice can be found in [7]).

We first carried out the harmonic analysis of the magnetic field data provided by [9] for the two ends of the magnets. Because of differing mechanical constraints the geometry of the two ends and the resulting fields are different. The two ends are referred to as 'Lead End' and 'Return End'. The magnetic field was calculated using a code that integrates the Biot-Savart law and approximates the effects of the iron yoke in the limit of infinite permeability.

The 2^{nd} and the 6^{th} harmonics for the Return End (the other harmonics of order lower than 6 are negligible) are shown in Figs. 3 and 4. From these harmonics one can recover the generalized gradients by applying the formulas reported in Section 3 and implemented in MARYLIE. In Fig. 5 we show the generalized gradient $C_{2,s}(z)$. In the pictures the fields are scaled by an arbitrary factor. Notice that the profile of $C_{2,s}(z)$ is smoother than the profile of $B_2(R,z)$. This is due to the contribution of the higher order

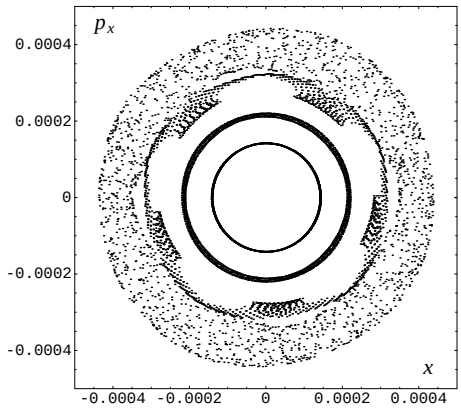

Figure 6: Projection of the Poincaré surface of section on the horizontal plane at the IP (normalized coordinates in units of $\mathrm{m}^{\frac{1}{2}}$). Map calculated from the magnetic field data.

derivatives of $C_{2,s}(z)$ to the field expansion [see Eq. (8)]. The integrated duodecapole component S_d of the fields at the two ends, defined by $S_d = \int_{END} C_{6,s}(z)dz$ was respectively 5.134×10^3 and 8.148×10^4 T/m^4 for the Return and Lead Ends.

Having computed the generalized gradients we calculated the transfer maps associated with the end regions and combined them with the transfer map for the body of the magnet to obtain the transfer map of the full quadrupole. By combining the transfer maps for the various elements in the IP region and the rest of the machine we constructed the one-turn map. This map we used for tracking studies.

Since the focus of our study was on the field modeling of the HG quadrupoles we considered a simplified version of the LHC lattice in which all the lattice elements, with the exception of the HG quadrupoles, were described in the linear approximation. Thus the only sources of nonlinearities (besides the purely geometric terms depending on the canonical momenta) were the intrinsic aberrations carried by the fringe fields [i.e. the 'pseudo-multipoles' or more specifically the aberrations generated by the terms $C_{2,s}^{[n]}$ with $n > 0$ in Eq. (8)] and the duodecapole field components at the HG magnet ends.

The result of a tracking study using this model is presented in Fig. 6, which shows the projection on the x-p_x plane of the Poincaré surface of section at one IP. The orbits of four particles are displayed over 10^5 turns, with the outer orbit being on the edge of the dynamic aperture. Tracking was done using the code CTRACK [10]. Normalized coordinates are used (*i.e.* $x_{norm} = x_{phys}/\sqrt{\beta_x}$ with $\beta_x = 0.5$ m, *etc.*). This picture should be compared to a similar projection of the Poincaré surface of section obtained with a model of the HG quadrupoles in which no duodecapole field components are present (see Fig. 7). One can observe the dynamic aperture increases by a factor of 5, suggesting that in the present design the duodecapole nonlinearities dominate over the intrinsic aberrations carried by

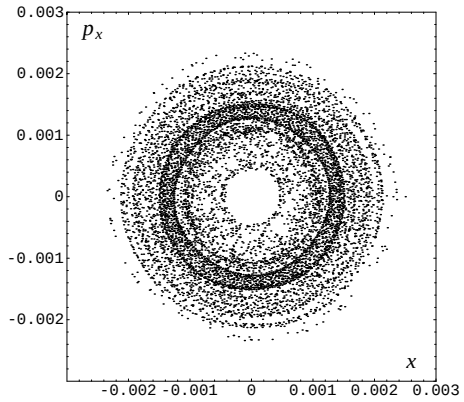

Figure 7: Projection of the Poincaré surface of section on the horizontal plane at the IP (normalized coordinates in units of $\mathrm{m}^{\frac{1}{2}}$). Map calculated from the magnetic field data with the duodecapoles turned off.

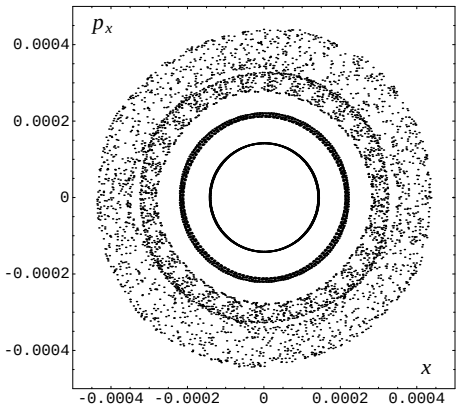

Figure 8: 'Standard model' for the HG quads: The quadrupole field component aberrations are treated in the hard edge limit and the systematic duodecapoles in the kick approximation. (Normalized coordinates in units of $\mathrm{m}^{\frac{1}{2}}$). To be compared with Fig. 6.

the quadrupole field components. And last Fig. 8 was obtained by tracking with a 'Standard Model' for quadrupole magnets. In this model the action of the duodecapole field components is approximated by thin kicks with strength S_d and the aberrations due to the quadrupole field components are evaluated though third order in the hard-edge limit. One can observe that the phase space portraits in the Figs. 6 and 8 are very similar. Since the nonlinearities are mostly due to the duodecapole field components the implication is that a thin kick approximation to model the duodecapole terms seems to be adequate. This is confirmed by an inspection of the Lie generators of the transfer map for an individual HG quadrupole in the two different models. In the Table below we show two such Lie generators. The generator x^6 is determined mostly by the duodecapole field components. The two values are within a few percents. On the other hand the generator x^2p_x, which measures the third order aberrations associated with the quadrupole field components, differs in the two cases by a factor 7. This shows that a more realistic modelling of the magnet fields may be necessary if the intrinsic quadrupole aberrations are found to be important.

Lie generator	Realistic Model	'Standard Model'
x^2p_x	0.54011D-04	0.72959D-03
x^6	-0.14337D+01	-0.13358D+01

6 ACKOWLEDGEMENTS

We have benefitted greatly from many conversations with P. Walstrom, the reading of some of his internal Technical Notes, and the use of his Fourier integration and Bessel function routines. We are also grateful to T. Mottershead, F. Neri, and P. Walstrom for their many contributions to MARYLIE 5.0. Finally, we thank G. Sabbi for providing us with magnetic field data for LHC quadrupoles. This work was supported by US Department of Energy Grant DEFG0296ER40949.

7 REFERENCES

[1] A. Dragt, Lie Methods for Nonlinear Dynamics with Applications to Accelerator Physics, University of Maryland Physics Department Report (1998).

[2] A. Dragt, F. Neri, G. Rangarajan, D. Douglas, L. Healy, and R. Ryne, Lie Algebraic Treatment of Linear and Nonlinear Beam Dynamics, Ann. Rev. Nucl. Part. Sci. **38** (1988) pp. 455-96.

[3] M. Venturini, A. Dragt, Accurate Computation of Transfer Maps from Magnetic Field Data, to be published in NIM-A.

[4] S. Caspi, M. Helm, and L.J. Laslett, The Use of Harmonics in 3-D Magnetic Fields, IEEE Trans. on Magnetics, vol.30, no. 4, (1994).

[5] M. Venturini, Lie Methods, Exact Map Computation and the Problem of Dispersion in Space Charge Dominated Beams, Ph. D. Dissertation (1998), Physics Department, University of Maryland.

[6] R. Trines, Modelling the Fringe Fields of a Multipole Device, Master Thesis (1998), Eindhoven University of Technology.

[7] The LHC lattice can be found on the Web at 'http://www-ap.fnal.gov/lhc/database/lattices'.

[8] G. Sabbi, HGQSO3 End Field Analysis, Fermilab Report TD-98-010 (1998).

[9] G. Sabbi, Private Communication.

[10] D. Abell, Analytic Properties and Cremona Approximation of Transfer Maps for Hamiltonian Systems, Ph. D Dissertation (1995), Physics Department, University of Maryland.